EUROPEAN ORGANIZATION FOR NUCLEAR RESEARCH

CERN-PPE/95-192
December 21, 1995

Study of the Structure of Hadronic Events and Determination of α_s at $\sqrt{s} = 130$ GeV and 136 GeV

L3 Collaboration

Abstract

We present a study of the structure of hadronic events recorded by the L3 detector at center-of-mass energies of 130 and 136 GeV. The data sample corresponds to an integrated luminosity of 5 pb^{-1} collected during the high energy run of 1995. The shapes of the event shape distributions and the energy dependence of their mean values are well reproduced by QCD models. From a comparison of the data with resummed $\mathcal{O}(\alpha_s^2)$ QCD calculations, we determine the strong coupling constant to be $\alpha_s(133 \text{ GeV}) = 0.107 \pm 0.005 \text{ (exp)} \pm 0.006 \text{ (theor)}$.

Submitted to *Phys. Lett. B*

Introduction

The theory of the strong interaction (QCD) [1] has been quite successful in describing many aspects of jet structure found in hadronic final states produced in e^+e^- annihilation, especially in hadronic Z decays [2]. Due to its nonabelian nature QCD predicts the strong coupling constant α_s to decrease with increasing energy. This characteristic is reflected in the energy dependence of the global structure of hadronic events. The 130-136 GeV e^+e^- annihilations produced at LEP at the end of 1995 have given a data set which is ideal to test QCD evolution predictions. We report on the studies of several event shape variables for these high energy hadronic final states. After corrections for detector effects and photon radiation the distributions are compared with QCD models which have been used extensively at $\sqrt{s} = 91$ GeV and for which the parameters have been tuned using hadronic Z decays. The energy dependence of the mean value of thrust and charge multiplicity measured at different center-of-mass energies ranging from 10 to 136 GeV is compared with QCD models.

The measured distributions of event shape variables at the two high center-of-mass energies have been combined and compared to the predictions of a second order QCD calculation with resummed leading and next-to-leading terms. This provides a determination of the strong coupling constant α_s at $\sqrt{s} = 133$ GeV. We use our previous α_s measurement at $\sqrt{s} = 91$ GeV [3,4] from a similar analysis to compare the relative change with the QCD expectation.

The L3 Detector

The L3 detector consists of a silicon microvertex detector, a central tracking chamber, a high resolution electromagnetic calorimeter composed of BGO crystals, a barrel of scintillation counters, a uranium hadron calorimeter with proportional wire chamber readout, and an accurate muon chamber system. These detectors are installed in a 12 m diameter magnet which provides a solenoidal field of 0.5 T and a toroidal field of 1.2 T. Luminosity is measured with a forward-backward BGO calorimeter on each side of the detector. A detailed description of each detector subsystem and its performance is given in [3,5].

The response of the L3 detector is modelled with the GEANT 3.15 [6] detector simulation program which includes the effects of energy loss, multiple scattering and showering in the detector materials and in the beam pipe.

Selection of Hadronic Events

For this analysis, we use events collected by the L3 detector at center-of-mass energies of $\sqrt{s} = 130.3$ and 136.3 GeV from the 1995 LEP high energy run, corresponding to a total integrated luminosity of 5 pb^{-1}.

The selection of $e^+e^- \to$ hadrons events is based on the energy measured in the electromagnetic and hadronic calorimeters.

We use energy clusters in the calorimeters with a minimum energy of 100MeV. We measure the total visible energy (E_{vis}) and the energy imbalances parallel ($E_{||}$) and perpendicular ($E_{\perp}$) to the beam direction. We select an event to be hadronic if the event satisfies the following cuts:

- $N_{cluster} > 13$ for $|\cos\theta_{thrust}| < 0.7$
- $N_{cluster} > 17$ for $|\cos\theta_{thrust}| > 0.7$

- $E_{vis}/\sqrt{s} > 0.5$
- $E_\perp/E_{vis} < 0.5$.

We select 953 and 675 hadronic events for $\sqrt{s} = 130$ and 136 GeV respectively.

Applying these cuts to fully simulated events we find that 96% of the hadronic events are accepted. Monte Carlo hadronic events were generated by the parton shower program PYTHIA5.7 [7] and passed through the L3 detector simulation. The main source of background is due to two-photon collisions ($e^+e^- \to e^+e^- +$ hadrons). Applying the same cuts to background Monte Carlo events produced by the PYTHIA generator [9] , the contamination in the selected hadron sample is estimated to be less than 4%.

The visible energy normalised to the center-of-mass energy of the selected events at 130 GeV is shown in figure 1. Taking into account experimental resolution effects, the visible energy distribution is consistent with a double peak structure. The two peaks correspond to perfectly balanced events at $E_{vis}/\sqrt{s} = 1$ and to hadronic Z decays with hard photons from initial state radiation escaping into the beam pipe ($E_{vis}/\sqrt{s} \approx 0.7$).

The fraction of events with hard initial state radiation (ISR) in our sample is about 75%. To reduce this contamination, the two following cuts have been applied:

- $(E_{vis}/\sqrt{s}) \ > \ 2.5(\mid E_{||} \mid /E_{vis}) + 0.5$
- energy of the most energetic $\gamma < 15$ GeV.

The first cut uses the correlation between $E_{vis}/\sqrt{s}$ and $\mid E_{||} \mid /E_{vis}$, which is shown in figure 2a. It discriminates well balanced events from unbalanced events arising from an ISR photon lost in the beam pipe. The well balanced events could contain initial state radiation where the photon is seen in the detector. These are removed by the second cut when a cluster compatible with a high energy photon of more than 15 GeV is found in the BGO calorimeter. Figure 2b shows the energy distribution of the most energetic photon in the BGO, where we observe a peak near 32 GeV corresponding to the ISR photon for the 130 GeV events.

The final sample used for this analysis contains 241 and 161 hadronic events for the 130 and 136 GeV samples respectively. After all the cuts the contamination from hard ISR (γ energy greater than 15 GeV) amounts to about 20% of the sample. This contamination affects the mean effective center-of-mass energy of the hadronic system which is lowered to about 125 GeV. The effect of ISR is accounted for using the PYTHIA Monte Carlo event generator. The remaining background due to $e^+e^- \to e^+e^- +$ hadrons is estimated to be less than 2%.

Definition and Measurement of the Observables

The jet structure of hadronic events can be analysed using global event shape variables. In this paper we limit our study to four variables for which improved QCD calculations are available [10–12]. We have previously measured these variables at $\sqrt{s} = 91$ GeV [3,13].

Thrust: The global event shape variable thrust, T, [14] is defined as:

$$T \ = \ \max \frac{\sum |\vec{p}_i \cdot \vec{n}_T|}{\sum |\vec{p}_i|} \ ,$$

where $\vec{p}_i$ is the momentum vector of the particle i. The thrust axis $\vec{n}_T$ is the unit vector which maximizes the above expression. The value of the thrust can vary between 0.5 and 1.

Scaled heavy jet mass: The heavy jet mass M_H is defined as: [15]

$$M_H = \max[M_+(\vec{n}_T), M_-(\vec{n}_T)] ,$$

where $M_\pm$ are the invariant masses in the two hemispheres, $S_\pm$, defined by the plane normal to the thrust axis:

$$M_\pm^2 = \left(\sum_{i\in S_\pm} p_i\right)^2$$

where p_i is the four momentum of particle i. The scaled heavy jet mass ρ is defined as:

$$\rho = M_H^2/s .$$

Jet broadening variables: These variables are defined [12] by computing in each hemisphere the quantity:

$$B_\pm = \frac{\sum_{i\in S_\pm} |\vec{p}_i \times \vec{n}_T|}{2\sum_i |\vec{p}_i|} .$$

The observables used to study α_s are

$$B_T = B_+ + B_- \quad \text{and} \quad B_W = \max(B_+, B_-)$$

referred to as 'total jet broadening' and 'wide jet broadening', respectively.

Jet multiplicity: Jets are reconstructed using the JADE algorithm [16]. For each pair of particles i and j the expression:

$$y_{ij} = \frac{2E_iE_j}{s} \cdot (1 - \cos\theta_{ij})$$

is evaluated. E_i and E_j are their energies and θ_{ij} is the angle between them. The pair for which y_{ij} is smallest is replaced by a pseudoparticle l with four-momentum

$$p_l = p_i + p_j .$$

This procedure is repeated until all y_{ij} exceed the jet resolution parameter y_{cut}. The remaining pseudoparticles are called jets. The jet fraction f_i is the fraction of all hadronic events containing i-jets

$$f_i = \frac{\sigma_{i-jets}}{\sigma_{tot}} .$$

f_i is a function of the jet resolution parameter y_{cut}.

Charge multiplicity: We define charge multiplicity, n_{ch}, as the number of charged particles per event.

The charge multiplicity distribution is obtained from reconstructed tracks while the other event shape distributions are obtained from reconstructed calorimetric clusters which are considered as massless particles. In the above definitions we replace the center-of-mass energy $\sqrt{s}$ by the measured energy sum of all clusters. For Monte Carlo events, the global event shape variables are calculated before (particle level) and after (detector level) detector simulation.

The calculation before the detector simulation takes into account all stable charged and neutral particles. The measured distributions at detector level differ from the ones at particle level because of detector effects, limited acceptance and finite resolution.

In Figure 3, the measured distributions for thrust and the jet fraction at $\sqrt{s} = 130$ GeV are compared with the PYTHIA predictions at detector level. Data and Monte Carlo are in agreement.

After subtracting the background events the distributions are corrected for detector effects, acceptance and resolution bin by bin comparing the detector level result with the particle level result for the same event sample. These correction factors are around 1 and have a maximum spread of 20%. We correct for initial and final state photon radiation bin by bin using Monte Carlo distributions at particle level with and without radiation. These correction factors are large and can vary even by a factor of 3 to 4 over the entire range. This unfolding procedure is sufficiently accurate considering the limited statistics of the data sample. We correct the charge multiplicity distribution assuming all weakly decaying light particles (K^0_s, Λ, etc. with mean lifetime larger than 3.3×10^{-10} s) to be stable.

Figure 4 shows the corrected thrust and scaled heavy jet mass distributions. The data are compared with PYTHIA 5.7 [7], HERWIG 5.6 [17] and ARIADNE 4.06 [18] QCD models at particle level without ISR . The three models agree with the measurements for the four observables T, ρ, B_T and B_W.

The largest systematic error comes from correction due to initial state radiation. In order to estimate its magnitude the ISR content in the event sample has been varied. The uncertainty corresponds to the difference between the result obtained with all the cuts with the result obtained after removing the cut on the visible photon in the detector. In this case the ISR contamination is increased from 20% to 40%. The systematic error estimated in this way is two to three times smaller than the statistical error.

Energy Dependences of the Mean Values

An important test of the QCD models is to check the predicted energy evolution of the shape distributions using the same Monte Carlo parameter values. The mean values of thrust and charged multiplicity are shown in figure 5, together with measurements at the Z resonance [13,19] as well as those at low energy e^+e^- machines [20]. Also shown are the energy dependences of these quantities as predicted by JETSET 7.4 PS [8], HERWIG 5.6, ARIADNE 4.06, COJETS 6.23 [21] and JETSET 7.4 ME Monte Carlo models with constant parameter values over the full energy range [13]. These models use different approaches to describe the perturbative and non perturbative phase of QCD evolution. For the thrust distribution all the models agree above 90 GeV. They are also in good agreement with the present measurement at 130 and 136 GeV. For the charge multiplicity the situation is different. ARIADNE does not reproduce the data but follows the evolution correctly. It should be noticed that ARIADNE as well as the other models has been tuned from global event shape distributions at 91 GeV [13] without the use of particle multiplicity distributions. The JETSET 7.4 ME model fails to describe the energy dependence of $< n_{ch} >$ over a wide energy range. This is understood as a consequence of a low parton multiplicity before fragmentation compared to the other models.

Since the present analysis is simpler than our previous one [13], the analysis has been repeated with a sample of data taken at $\sqrt{s} = 91$ GeV and the results are compared. The difference between these two analyses is used to estimate the systematic error on the mean values.

The measured mean values of thrust, scaled heavy jet mass, total jet broadening, wide jet broadening and charge multiplicity at 130 and 136 GeV are summarised in table 1.

QCD Predictions

QCD predictions in fixed second order perturbation theory cannot take into account the effect of multiple gluon emission. For variables like thrust, heavy jet mass, etc. this leads to a singular behavior of the distributions in kinematic regions where multi-gluon emission becomes dominant. This is a direct consequence of the collinear and infrared divergence of the gluon emission cross section. It is possible to isolate the singular terms in every order of the perturbation series and to sum them up in the form of an exponential. These calculations have been carried out for the variables $1-T$, ρ, B_T, B_W (denoted generically by y) to next-to-leading log terms [10–12]. On the other hand, in the fixed order calculations [22,23], all the contributions (including the subleading terms) are summed to second order. In order to describe the data over a wide kinematic range, it is desirable to combine the two sets of calculations taking care of the common parts.

This leads to a number of matching schemes. A prefered approach to combine the two calculations is to take the log of the fixed order calculations, to expand it as a power series and to subtract out the leading and next-to-leading terms from the second order calculation. In addition, one needs to satisfy the kinematic constraints, namely the cross sections vanish beyond the kinematic limits. This can be achieved by replacing the variable y in the resummed terms by $(y^{-1} - y_{\mathrm{max}}^{-1} + 1)^{-1}$ [24].

An important improvement of the new QCD calculations with respect to the second order formulae is their ability to describe also the low y region. These calculations are given in the form of analytical functions for massless partons: $f^{\mathrm{pert}}(y; s, \alpha_{\mathrm{s}}(\mu), \mu)$.

To compare the analytical calculations with the experimental distributions, one has to include the effect of hadronization and decays using Monte Carlo programs. We have used the parton shower programs JETSET 7.4 PS, ARIADNE 4.06, HERWIG 5.6 and NLLJET 2.0 [25] with string or cluster fragmentation. The fragmentation parameters are determined from a comparison of predicted and measured distributions for several event shape variables [13, 26]. All these generators describe our experimental measurements well. We fold the perturbative calculations for a variable y with the probability $p^{\mathrm{non-pert}}\ (y',y)$ to find a value y after fragmentation and decays for a parton level value y':

$$f(y) = \int f^{\mathrm{pert}}(y') \cdot p^{\mathrm{non-pert}}(y', y)\, dy' \ .$$

We compare the resulting differential cross section $f(y)$ to our measurements. The correction for hadronization and decays changes the perturbative prediction by less than 5% for the event shape variables over a large kinematic range. The corrections increase in the extreme two jet region.

We estimate the uncertainties in the probabilities $p^{\mathrm{non-pert}}(y', y)$ and the corresponding error in α_{s} by:

- changing the fragmentation parameters in the JETSET model,
- comparing the predictions of the different hadronization models.

Since the variables used are affected differently by higher order effects and hadronization corrections, a comparison of the corresponding α_{s} values allows an estimate of the size of theoretical uncertainties.

Results

In order to derive α_s, we fit the theoretical distribution $f(y)$ to the measured event shape distributions for a fixed scale $\mu = \sqrt{s}$. The experimental distributions are the weighted average of the distributions obtained at the two center-of-mass energies because the two energies are close enough.

For the fit we use the ranges as given in table 2. The choice of these ranges account for the following factors:

- reliability of the resummation calculation,
- smallness and uniformity of detector and hadronization corrections,
- sufficient statistics.

Figures 6(a-d) show the experimental data together with the QCD fits for the four variables thrust, scaled heavy jet mass, total and wide jet broadening. The results in table 3 are the α_s values as obtained from the fits to $\mathcal{O}(\alpha_s^2)$ + resummed calculations using hadronization corrections from JETSET with standard L3 parameters [13] together with the χ^2 values.

The errors also shown in table 3 are divided into three main parts. The first part corresponds to the statistical errors together with the experimental systematic uncertainties estimated by changing the ISR contamination before corrections.

The second part shows the variation in the fitted value of α_s with respect to JETSET due to the use of different hadronization models and the overall variation due to the parameter changes in JETSET, the dominant contribution being the Bose-Einstein effect. For all variables, except the scaled heavy jet mass, the most important variation comes from the different fragmentation models. We use this as an estimate of the overall hadronization uncertainty.

The third part summarizes the errors coming from uncalculated higher orders in the QCD predictions. The scale error is obtained by repeating the α_s fit for different values of the renormalization scale in the interval $0.5\sqrt{s} \leq \mu \leq 2\sqrt{s}$. For all these scales a good fit is obtained. The matching scheme uncertainty is obtained from half of the maximum spread due to the variation of the matching algorithm. The systematic errors due to uncalculated higher order terms have been estimated independently from the scale uncertainty and the matching scheme uncertainty. The largest of these is taken as the theoretical uncertainty due to uncalculated higher orders. The overall theoretical error is obtained by adding to this in quadrature the hadronization uncertainty.

The α_s values from the four distributions are affected differently by higher order corrections and hadronization effects. To obtain a combined value for the strong coupling constant we take the unweighted average of the four α_s values of table 3 and obtain $\alpha_s = 0.107 \pm 0.005\,(\mathrm{exp})$. We conservatively assign the overall theoretical uncertainty as the average of the four theoretical errors. The combined result is

$$\alpha_s(133 \text{ GeV}) = 0.107 \pm 0.005 \pm 0.006$$

where the first error is experimental and the second error is theoretical. Extrapolating the α_s value from μ=133 GeV to M_Z assuming the energy dependence as predicted by QCD with five quark flavours [27] gives:

$$\alpha_s(M_Z) = 0.113 \pm 0.006 \pm 0.007$$

This may be compared with our earlier measurement [4] of $\alpha_s(M_Z) = 0.125 \pm 0.003 \pm 0.008$ from a study of event shape variables in hadronic Z decays at $\sqrt{s} = M_Z$. These two measurements are consistent with the energy evolution predicted by QCD within 1.5 σ.

Conclusions

We have studied a number of event shape variables from the sample of hadronic events produced in e^+e^- annihilation at $\sqrt{s} = 130$ GeV and 136 GeV. The global structure of these events is well reproduced by several Monte Carlo models, based on parton shower evolution, together with string or cluster fragmentation and with parameters adjusted from hadronic Z decays at $\sqrt{s} = 91$ GeV. We have also studied the energy evolution of the mean values of thrust and charge multiplicity which show the predicted QCD evolution. From a fit of the second order QCD calculation with resummed leading and next-to-leading terms to the thrust, scaled heavy jet mass, total jet broadening and wide jet broadening distributions, obtained from the complete sample of 130 to 136 GeV events, we determine the strong coupling constant:

$$\alpha_s(133 \text{ GeV}) = 0.107 \pm 0.005 \text{ (exp)} \pm 0.006 \text{ (theor)}$$

The first error is the experimental uncertainty which is dominated by statistics. The second error is due to hadronization uncertainties and approximations in the calculation of the higher order corrections.

Acknowledgements

We wish to congratulate the CERN accelerator divisions for the successful upgrade of the LEP machine and to express our gratitude for the excellent performance of the machine. We acknowledge with appreciation the effort of all engineers, technicians and support staff who have participated in the construction and maintenance of this experiment. Those of us who are not from member states thank CERN for its hospitality and help.

References

[1] M. Gell-Mann, Acta Phys. Austriaca Suppl. **IX** (1972) 733;
H. Fritzsch and M. Gell-Mann, 16th International Conference on High Energy Physics, Batavia, 1972; editors J.D. Jackson and A. Roberts, National Accelerator Laboratory (1972);
H. Fritzsch, M. Gell-Mann and H. Leytwyler, Phys. Lett. **B 47** (1973) 365;
D.J. Gross and F. Wilczek, Phys. Rev. Lett. **30** (1973) 1343;
D.J. Gross and F. Wilczek, Phys. Rev. **D8** (1973) 3633;
H.D. Politzer, Phys. Rev. Lett. **30** (1973) 1346;
G. 't Hooft, Nucl. Phys. **B33** (1971) 173.

[2] T. Hebbeker, Phys. Rep. **Vol.217** (1992) 69;
S.Bethke, J.E. Pilcher, Ann. Rev. Nucl. Part. Sci. **42** (1992) 251;
M. Schmelling, CERN/PPE 94-184, submitted to Physica Scripta.

[3] L3 Collaboration, O. Adriani *et al.*, Phys. Rep., **236** (1993) 1.

[4] L3 Collaboration, O. Adriani *et al.*, Phys. Lett. **B284** (1992) 471.

[5] L3 Collaboration, B. Adeva *et al.*, Nucl. Inst. Meth. **A 289** (1990) 35;
L3 Collaboration, M. Acciari *et al.*, Nucl. Inst. Meth. **A 351** (1994) 300.

[6] The L3 detector simulation is based on GEANT Version 3.15.
See R. Brun *et al.*, "GEANT 3", CERN DD/EE/84-1 (Revised), September 1987.
The GHEISHA program (H. Fesefeldt, RWTH Aachen Report PITHA 85/02 (1985)) is used to simulate hadronic interactions.

[7] PYTHIA 5.7 Monte Carlo Program:
QCD parton shower and fragmentation process are taken from JETSET 7.4 [8];
T. Sjöstrand, CERN-TH-7112/93 (1993), revised august 1995;
T. Sjöstrand, Comp. Phys. Comm. **82** (1994) 74.

[8] JETSET 7.4 Monte Carlo Program:
T. Sjöstrand, Comp. Phys. Comm. **39** (1986) 347;
T. Sjöstrand and M. Bengtsson, Comp. Phys. Comm. **43** (1987) 367.

[9] G.A. Schuler and T. Sjöstrand, Nucl. Phys. **B407** (1993) 539; Phys. Lett. **B300** (1993) 169.
The Monte Carlo program used for two-photon processes is incorporated in PYTHIA 5.7 [7].

[10] S. Catani *et al.*, Phys. Lett. **B263** (1991) 491.

[11] S. Catani *et al.*, Phys. Lett. **B272** (1991) 360.

[12] S. Catani *et al.*, Phys. Lett. **B295** (1992) 269.

[13] L3 Collaboration, B. Adeva *et al.*, Z. Phys. **C55** (1992) 39.

[14] S. Brandt *et al.*, Phys. Lett. **12** (1964) 57;
E. Fahri, Phys. Rev. Lett. **39** (1977) 1587.

[15] T. Chandramohan and L. Clavelli, Nucl. Phys. **B184** (1981) 365;
MARK II Collaboration, A. Peterson *et al.*, Phys. Rev. **D 37** (1988) 1;
TASSO Collaboration, W. Braunschweig *et al.*, Z. Phys. **C45** (1989) 11.

[16] JADE Collaboration, W. Bartel *et al.*, Z. Phys. **C33** (1986) 23;
JADE Collaboration,S. Bethke *et al.*, Phys. Lett. **B213** (1988) 235.

[17] HERWIG 5.6 Monte Carlo Program:
G. Marchesini and B. Webber, Nucl. Phys. **B310** (1988) 461;
I.G. Knowles, Nucl. Phys. **B310** (1988) 571;
G. Marchesini *et al.*, Comp. Phys. Comm. **67** (1992) 465.

[18] ARIADNE 4.06 Monte Carlo Program:
U. Pettersson, "ARIADNE: A Monte Carlo for QCD Cascades in the Color Dipole Formulation", Lund Preprint, LU TP 88-5 (1988);
L. Lönnblad, "The Colour Dipole Cascade Model and the Ariadne Program", Lund Preprint, LU TP 91-11 (1991).

[19] ALEPH Collaboration, D. Decamp *et al.*, Phys. Lett. **B273** (1991) 181;
DELPHI Collaboration, P. Aarnio *et al.*, Phys. Lett. **B240** (1990) 271;
DELPHI Collaboration, P. Abreu *et al.*, Z. Phys. **C50** (1991) 185;
OPAL Collaboration, M.Z. Akrawy *et al.*, Z. Phys. **C47** (1990) 505;
OPAL Collaboration, P.D. Acton *et al.*, Z. Phys. **C53** (1992) 539.

[20] AMY Collaboration, Y.K. Li *et al.*, Phys. Rev. **D41** (1990) 2675;
AMY Collaboration, H.W. Zheng *et al.*, Phys. Rev. **D42** (1990) 737;
JADE Collaboration, W. Bartel *et al.*, Z. Phys. **C20** (1983) 187;
MARK J Collaboration, D.P. Barber *et al.*, Phys. Rev. Lett. **43** (1979) 901;
TASSO Collaboration, W. Braunschweig *et al.*, Z. Phys. **C45** (1989) 193;
TASSO Collaboration, W. Braunschweig *et al.*, Z. Phys. **C47** (1990) 187;
M. Yamauchi (TOPAZ Collaboration), "Recent Results from TOPAZ at TRISTAN", 24th Int. Conf. on High Energy Physics, Munich 1988.

[21] COJETS 6.23 Monte Carlo Program:
R. Odorico, Nucl. Phys. **B228** (1983) 381;
R. Odorico, Comp. Phys. Comm. **32** (1984) 139, Erratum: **34** (1985) 43;
R. Mazzanti and R. Odorico, Nucl. Phys. **B370** (1992) 23; Bologna preprint DFUB 92/1.

[22] R.K. Ellis, D.A. Ross and A.E. Terrano, Nucl. Phys. **B178** (1981) 421.

[23] Z. Kunszt and P. Nason in "Z Physics at LEP 1", CERN Report 89-08, Vol.I., p. 373.

[24] S. Catani *et al.*, Nucl. Phys. **B407** (1993) 3.

[25] NLLJET 2.0 Monte Carlo Program:
K. Kato and T. Munehisa, Phys. Rev. **D36** (1987) 61;
K. Kato and T. Munehisa, Comp. Phys. Comm. **64** (1991) 67.

[26] L3 Collaboration, B. Adeva *et al.*, Phys. Lett. **B241** (1990) 416;
L3 Collaboration, B. Adeva *et al.*, Phys. Lett. **B261** (1991) 177.

[27] Particle Data Group, L. Montanet *et al.*, Phys. Rev. **D50** (1994) 1773.

The L3 Collaboration:

M.Acciarri,[29] A.Adam,[48] O.Adriani,[18] M.Aguilar-Benitez,[28] S.Ahlen,[12] B.Alpat,[36] J.Alcaraz,[28] J.Allaby,[19] A.Aloisio,[31] G.Alverson,[13] M.G.Alviggi,[31] G.Ambrosi,[36] H.Anderhub,[51] V.P.Andreev,[40] T.Angelescu,[14] D.Antreasyan,[10] A.Arefiev,[30] T.Azemoon,[3] T.Aziz,[11] P.Bagnaia,[39,19] L.Baksay,[46] R.C.Ball,[3] S.Banerjee,[11] K.Banicz,[48] R.Barillère,[19] L.Barone,[39] P.Bartalini,[36] A.Baschirotto,[29] M.Basile,[10] R.Battiston,[36] A.Bay,[24] F.Becattini,[18] U.Becker,[17] F.Behner,[51] Gy.L.Bencze,[15] J.Berdugo,[28] P.Berges,[17] B.Bertucci,[19] B.L.Betev,[51] M.Biasini,[19] A.Biland,[51] G.M.Bilei[36] J.J.Blaising,[19] S.C.Blyth,[37] G.J.Bobbink,[2] R.Bock,[1] A.Böhm,[1] B.Borgia,[39] A.Boucham,[4] D.Bourilkov,[51] M.Bourquin,[21] D.Boutigny,[4] E.Brambilla,[17] J.G.Branson,[42] V.Brigljevic,[51] I.C.Brock,[37] A.Buijs,[47] A.Bujak,[48] J.D.Burger,[17] W.J.Burger,[21] C.Burgos,[28] J.Busenitz,[46] A.Buytenhuijs,[33] X.D.Cai,[20] M.Campanelli,[51] M.Capell,[17] G.Cara Romeo,[10] M.Caria,[36] G.Carlino,[4] A.M.Cartacci,[18] J.Casaus,[28] G.Castellini,[18] R.Castello,[29] F.Cavallari,[39] N.Cavallo,[31] C.Cecchi,[21] M.Cerrada,[28] F.Cesaroni,[25] M.Chamizo,[28] A.Chan,[53] Y.H.Chang,[53] U.K.Chaturvedi,[20] M.Chemarin,[27] A.Chen,[53] C.Chen,[8] G.Chen,[8] G.M.Chen,[8] H.F.Chen,[22] H.S.Chen,[8] X.Chereau,[4] G.Chiefari,[31] C.Y.Chien,[5] M.T.Choi,[45] L.Cifarelli,[41] F.Cindolo,[10] C.Civinini,[18] I.Clare,[17] R.Clare,[17] T.E.Coan,[26] H.O.Cohn,[34] G.Coignet,[4] A.P.Colijn,[2] N.Colino,[28] V.Commichau,[1] S.Costantini,[39] F.Cotorobai,[14] B.de la Cruz,[28] T.S.Dai,[17] R.D'Alessandro,[18] R.de Asmundis,[31] H.De Boeck,[33] A.Degré,[4] K.Deiters,[49] E.Dénes,[15] P.Denes,[38] F.DeNotaristefani,[39] D.DiBitonto,[46] M.Diemoz,[39] D.van Dierendonck,[2] F.Di Lodovico,[51] C.Dionisi,[39] M.Dittmar,[51] A.Dominguez,[42] A.Doria,[31] I.Dorne,[4] M.T.Dova,[20,♯] E.Drago,[31] D.Duchesneau,[4] P.Duinker,[2] I.Duran,[43] S.Dutta,[11] S.Easo,[36] Yu.Efremenko,[34] H.El Mamouni,[27] A.Engler,[37] F.J.Eppling,[17] F.C.Erné,[2] J.P.Ernenwein,[27] P.Extermann,[21] R.Fabbretti,[49] M.Fabre,[49] R.Faccini,[39] S.Falciano,[39] A.Favara,[18] J.Fay,[27] M.Felcini,[51] T.Ferguson,[37] D.Fernandez,[28] G.Fernandez,[28] F.Ferroni,[39] H.Fesefeldt,[1] E.Fiandrini,[36] J.H.Field,[21] F.Filthaut,[37] P.H.Fisher,[17] G.Forconi,[17] L.Fredj,[21] K.Freudenreich,[51] M.Gailloud,[24] Yu.Galaktionov,[30,17] S.N.Ganguli,[11] P.Garcia-Abia,[28] S.S.Gau,[13] S.Gentile,[39] J.Gerald,[5] N.Gheordanescu,[14] S.Giagu,[39] S.Goldfarb,[24] J.Goldstein,[12] Z.F.Gong,[22] E.Gonzalez,[28] A.Gougas,[5] D.Goujon,[21] G.Gratta,[35] M.W.Gruenewald,[9] V.K.Gupta,[38] A.Gurtu,[11] H.R.Gustafson,[3] L.J.Gutay,[48] K.Hangarter,[1] B.Hartmann,[1] A.Hasan,[32] J.T.He,[8] T.Hebbeker,[9] A.Hervé,[19] W.C.van Hoek,[33] H.Hofer,[51] H.Hoorani,[21] S.R.Hou,[53] G.Hu,[20] M.M.Ilyas,[20] V.Innocente,[19] H.Janssen,[4] B.N.Jin,[8] L.W.Jones,[3] P.de Jong,[17] I.Josa-Mutuberria,[28] A.Kasser,[24] R.A.Khan,[20] Yu.Kamyshkov,[34] P.Kapinos,[50] J.S.Kapustinsky,[26] Y.Karyotakis,[4] M.Kaur,[20,◇] M.N.Kienzle-Focacci,[21] D.Kim,[5] J.K.Kim,[45] S.C.Kim,[45] Y.G.Kim,[45] W.W.Kinnison,[26] A.Kirkby,[35] D.Kirkby,[35] J.Kirkby,[19] W.Kittel,[33] A.Klimentov,[17,30] A.C.König,[33] E.Koffeman,[2] A.Köngeter,[1] V.Koutsenko,[17,30] A.Koulbardis,[40] R.W.Kraemer,[37] T.Kramer,[17] W.Krenz,[1] H.Kuijten,[33] A.Kunin,[17,30] P.Ladron de Guevara,[28] G.Landi,[18] C.Lapoint,[17] K.Lassila-Perini,[51] P.Laurikainen,[23] M.Lebeau,[19] A.Lebedev,[17] P.Lebrun,[27] P.Lecomte,[51] P.Lecoq,[19] P.Le Coultre,[51] J.S.Lee,[45] K.Y.Lee,[45] C.Leggett,[3] J.M.Le Goff,[19] R.Leiste,[50] M.Lenti,[18] E.Leonardi,[39] P.Levtchenko,[40] C.Li,[22] E.Lieb,[50] W.T.Lin,[53] F.L.Linde,[2] B.Lindemann,[1] L.Lista,[31] Z.A.Liu,[8] W.Lohmann,[50] E.Longo,[39] W.Lu,[35] Y.S.Lu,[8] K.Lübelsmeyer,[1] C.Luci,[39] D.Luckey,[17] L.Ludovici,[39] L.Luminari,[39] W.Lustermann,[49] W.G.Ma,[22] A.Macchiolo,[18] M.Maity,[11] G.Majumder,[11] L.Malgeri,[39] A.Malinin,[30] C.Maña,[28] S.Mangla,[11] M.Maolinbay,[51] P.Marchesini,[51] A.Marin,[12] J.P.Martin,[27] F.Marzano,[39] G.G.G.Massaro,[2] K.Mazumdar,[11] D.McNally,[19] R.R.McNeil,[7] S.Mele,[31] L.Merola,[31] M.Meschini,[18] W.J.Metzger,[33] M.von der Mey,[1] Y.Mi,[24] A.Mihul,[14] A.J.W.van Mil,[33] G.Mirabelli,[39] J.Mnich,[19] M.Möller,[1] B.Monteleoni,[18] R.Moore,[3] S.Morganti,[39] R.Mount,[35] S.Müller,[1] F.Muheim,[21] E.Nagy,[15] S.Nahn,[17] M.Napolitano,[31] F.Nessi-Tedaldi,[51] H.Newman,[35] A.Nippe,[1] H.Nowak,[50] G.Organtini,[39] R.Ostonen,[23] D.Pandoulas,[1] S.Paoletti,[39] P.Paolucci,[31] H.K.Park,[37] G.Pascale,[39] G.Passaleva,[18] S.Patricelli,[31] T.Paul,[36] M.Pauluzzi,[36] C.Paus,[1] F.Pauss,[51] Y.J.Pei,[1] S.Pensotti,[29] D.Perret-Gallix,[4] S.Petrak,[9] A.Pevsner,[5] D.Piccolo,[31] M.Pieri,[18] J.C.Pinto,[37] P.A.Piroué,[38] E.Pistolesi,[18] V.Plyaskin,[30] M.Pohl,[51] V.Pojidaev,[30,18] H.Postema,[17] N.Produit,[21] R.Raghavan,[11] G.Rahal-Callot,[51] P.G.Rancoita,[29] M.Rattaggi,[29] G.Raven,[42] P.Razis,[32] K.Read,[34] M.Redaelli,[29] D.Ren,[51] M.Rescigno,[39] S.Reucroft,[13] A.Ricker,[1] S.Riemann,[50] B.C.Riemers,[48] K.Riles,[3] O.Rind,[3] S.Ro,[45] A.Robohm,[51] J.Rodin,[17] F.J.Rodriguez,[28] B.P.Roe,[3] S.Röhner,[1] L.Romero,[28] S.Rosier-Lees,[4] Ph.Rosselet,[24] W.van Rossum,[47] S.Roth,[1] J.A.Rubio,[19] H.Rykaczewski,[51] J.Salicio,[19] J.M.Salicio,[28] E.Sanchez,[28] A.Santocchia,[36] M.E.Sarakinos,[23] S.Sarkar,[11] M.Sassowsky,[1] C.Schäfer,[1] V.Schegelsky,[40] S.Schmidt-Kaerst,[1] D.Schmitz,[1] P.Schmitz,[1] M.Schneegans,[4] B.Schoeneich,[50] N.Scholz,[51] H.Schopper,[52] D.J.Schotanus,[33] R.Schulte,[1] K.Schultze,[1] J.Schwenke,[1] G.Schwering,[1] C.Sciacca,[31] P.G.Seiler,[49] J.C.Sens,[53] L.Servoli,[36] S.Shevchenko,[35] N.Shivarov,[44] V.Shoutko,[30] J.Shukla,[26] E.Shumilov,[30] T.Siedenburg,[1] D.Son,[45] A.Sopczak,[50] V.Soulimov,[31] B.Smith,[17] P.Spillantini,[18] M.Steuer,[17] D.P.Stickland,[38] F.Sticozzi,[17] H.Stone,[38] B.Stoyanov,[44] A.Straessner,[1] K.Strauch,[16] K.Sudhakar,[11] G.Sultanov,[20] L.Z.Sun,[22] G.F.Susinno,[21] H.Suter,[51] J.D.Swain,[20] X.W.Tang,[8] L.Tauscher,[6] L.Taylor,[13] Samuel C.C.Ting,[17] S.M.Ting,[17] O.Toker,[36] F.Tonisch,[50] M.Tonutti,[1] S.C.Tonwar,[11] J.Tóth,[15] A.Tsaregorodtsev,[40] C.Tully,[38] H.Tuchscherer,[46] K.L.Tung,[8] J.Ulbricht,[51] L.Urbán,[15] U.Uwer,[19] E.Valente,[39] R.T.Van de Walle,[33] I.Vetlitsky,[30] G.Viertel,[51] M.Vivargent,[4] R.Völkert,[50] H.Vogel,[37] H.Vogt,[50] I.Vorobiev,[30] A.A.Vorobyov,[40] An.A.Vorobyov,[40] L.Vuilleumier,[24] M.Wadhwa,[6] W.Wallraff,[1] J.C.Wang,[17] X.L.Wang,[22] Y.F.Wang,[17] Z.M.Wang,[22] A.Weber,[1] R.Weill,[24] C.Willmott,[28] F.Wittgenstein,[19] S.X.Wu,[20] S.Wynhoff,[1] J.Xu,[12] Z.Z.Xu,[22] B.Z.Yang,[22] C.G.Yang,[8] X.Y.Yao,[8] J.B.Ye,[22] S.C.Yeh,[53] J.M.You,[37] C.Zaccardelli,[35] An.Zalite,[40] P.Zemp,[51] J.Y.Zeng,[8] Y.Zeng,[1] Z.Zhang,[8] Z.P.Zhang,[22] B.Zhou,[12] G.J.Zhou,[8] Y.Zhou,[3] G.Y.Zhu,[8] R.Y.Zhu,[35] A.Zichichi,[10,19,20] B.C.C.van der Zwaan.[2]

1 I. Physikalisches Institut, RWTH, D-52056 Aachen, FRG[§]
III. Physikalisches Institut, RWTH, D-52056 Aachen, FRG[§]
2 National Institute for High Energy Physics, NIKHEF, and University of Amsterdam, NL-1009 DB Amsterdam, The Netherlands
3 University of Michigan, Ann Arbor, MI 48109, USA
4 Laboratoire d'Annecy-le-Vieux de Physique des Particules, LAPP,IN2P3-CNRS, BP 110, F-74941 Annecy-le-Vieux CEDEX, France
5 Johns Hopkins University, Baltimore, MD 21218, USA
6 Institute of Physics, University of Basel, CH-4056 Basel, Switzerland
7 Louisiana State University, Baton Rouge, LA 70803, USA
8 Institute of High Energy Physics, IHEP, 100039 Beijing, China
9 Humboldt University, D-10099 Berlin, FRG[§]
10 INFN-Sezione di Bologna, I-40126 Bologna, Italy
11 Tata Institute of Fundamental Research, Bombay 400 005, India
12 Boston University, Boston, MA 02215, USA
13 Northeastern University, Boston, MA 02115, USA
14 Institute of Atomic Physics and University of Bucharest, R-76900 Bucharest, Romania
15 Central Research Institute for Physics of the Hungarian Academy of Sciences, H-1525 Budapest 114, Hungary[‡]
16 Harvard University, Cambridge, MA 02139, USA
17 Massachusetts Institute of Technology, Cambridge, MA 02139, USA
18 INFN Sezione di Firenze and University of Florence, I-50125 Florence, Italy
19 European Laboratory for Particle Physics, CERN, CH-1211 Geneva 23, Switzerland
20 World Laboratory, FBLJA Project, CH-1211 Geneva 23, Switzerland
21 University of Geneva, CH-1211 Geneva 4, Switzerland
22 Chinese University of Science and Technology, USTC, Hefei, Anhui 230 029, China
23 SEFT, Research Institute for High Energy Physics, P.O. Box 9, SF-00014 Helsinki, Finland
24 University of Lausanne, CH-1015 Lausanne, Switzerland
25 INFN-Sezione di Lecce and Universitá Degli Studi di Lecce, I-73100 Lecce, Italy
26 Los Alamos National Laboratory, Los Alamos, NM 87544, USA
27 Institut de Physique Nucléaire de Lyon, IN2P3-CNRS,Université Claude Bernard, F-69622 Villeurbanne, France
28 Centro de Investigaciones Energeticas, Medioambientales y Tecnologicas, CIEMAT, E-28040 Madrid, Spain[♭]
29 INFN-Sezione di Milano, I-20133 Milan, Italy
30 Institute of Theoretical and Experimental Physics, ITEP, Moscow, Russia
31 INFN-Sezione di Napoli and University of Naples, I-80125 Naples, Italy
32 Department of Natural Sciences, University of Cyprus, Nicosia, Cyprus
33 University of Nymegen and NIKHEF, NL-6525 ED Nymegen, The Netherlands
34 Oak Ridge National Laboratory, Oak Ridge, TN 37831, USA
35 California Institute of Technology, Pasadena, CA 91125, USA
36 INFN-Sezione di Perugia and Universitá Degli Studi di Perugia, I-06100 Perugia, Italy
37 Carnegie Mellon University, Pittsburgh, PA 15213, USA
38 Princeton University, Princeton, NJ 08544, USA
39 INFN-Sezione di Roma and University of Rome, "La Sapienza", I-00185 Rome, Italy
40 Nuclear Physics Institute, St. Petersburg, Russia
41 University and INFN, Salerno, I-84100 Salerno, Italy
42 University of California, San Diego, CA 92093, USA
43 Dept. de Fisica de Particulas Elementales, Univ. de Santiago, E-15706 Santiago de Compostela, Spain
44 Bulgarian Academy of Sciences, Central Laboratory of Mechatronics and Instrumentation, BU-1113 Sofia, Bulgaria
45 Center for High Energy Physics, Korea Advanced Inst. of Sciences and Technology, 305-701 Taejon, Republic of Korea
46 University of Alabama, Tuscaloosa, AL 35486, USA
47 Utrecht University and NIKHEF, NL-3584 CB Utrecht, The Netherlands
48 Purdue University, West Lafayette, IN 47907, USA
49 Paul Scherrer Institut, PSI, CH-5232 Villigen, Switzerland
50 DESY-Institut für Hochenergiephysik, D-15738 Zeuthen, FRG
51 Eidgenössische Technische Hochschule, ETH Zürich, CH-8093 Zürich, Switzerland
52 University of Hamburg, D-22761 Hamburg, FRG
53 High Energy Physics Group, Taiwan, China
§ Supported by the German Bundesministerium für Bildung, Wissenschaft, Forschung und Technologie
‡ Supported by the Hungarian OTKA fund under contract numbers 2970 and T14459.
♭ Supported also by the Comisión Interministerial de Ciencia y Technología
♮ Also supported by CONICET and Universidad Nacional de La Plata, CC 67, 1900 La Plata, Argentina
◇ Also supported by Panjab University, Chandigarh-160014, India

	$\sqrt{s} = 130$ GeV	$\sqrt{s} = 136$ GeV
$< T >$	$0.948 \pm 0.004 \pm 0.007$	$0.943 \pm 0.005 \pm 0.008$
$< \rho >$	$0.045 \pm 0.003 \pm 0.001$	$0.046 \pm 0.004 \pm 0.001$
$< B_T >$	$0.095 \pm 0.004 \pm 0.001$	$0.094 \pm 0.005 \pm 0.001$
$< B_W >$	$0.067 \pm 0.003 \pm 0.001$	$0.066 \pm 0.004 \pm 0.001$
$< n_{ch} >$	$24.9 \pm 0.5 \pm 0.8$	$24.2 \pm 0.7 \pm 0.8$

Table 1: Mean values of thrust, T, scaled heavy jet mass, ρ, total jet broadening, B_T, wide jet broadening, B_W, and charge multiplicity, n_{ch}, measured at $\sqrt{s} = 130$ and 136 GeV. The first error is statistical and the second is systematic.

Variable	Fit range
$(1-T)$	0.00 – 0.400
ρ	0.00 – 0.300
B_T	0.00 – 0.400
B_W	0.05 – 0.175

Table 2: Ranges used for QCD fits to the data

	$(1-T)$	ρ	B_T	B_W
$\alpha_s(133\ \mathrm{GeV})$	0.1094	0.1078	0.1071	0.1031
χ^2/d.o.f.	1.04	0.74	2.12	0.54
Statistical error	±0.0047	±0.0047	±0.0036	±0.0037
Systematic error	±0.0019	±0.0015	±0.0010	±0.0014
Overall experimental error	±0.0051	±0.0050	±0.0037	±0.0040
Fragmentation Model	$\pm$ 0.0069	$\pm$ 0.0025	$\pm$ 0.0059	$\pm$ 0.0038
Model parameters	±0.0037	±0.0032	±0.0026	±0.0016
Hadronization uncertainty	±0.0069	±0.0025	±0.0059	±0.0038
QCD scale uncertainty	±0.0022	±0.0016	±0.0026	±0.0018
Matching scheme uncertainty	±0.0016	±0.0018	±0.0053	±0.0043
Error due to higher orders	±0.0022	±0.0018	±0.0053	±0.0043
Overall theoretical error	±0.0072	±0.0031	±0.0079	±0.0057

Table 3: α_s from the fits to the event shape variables

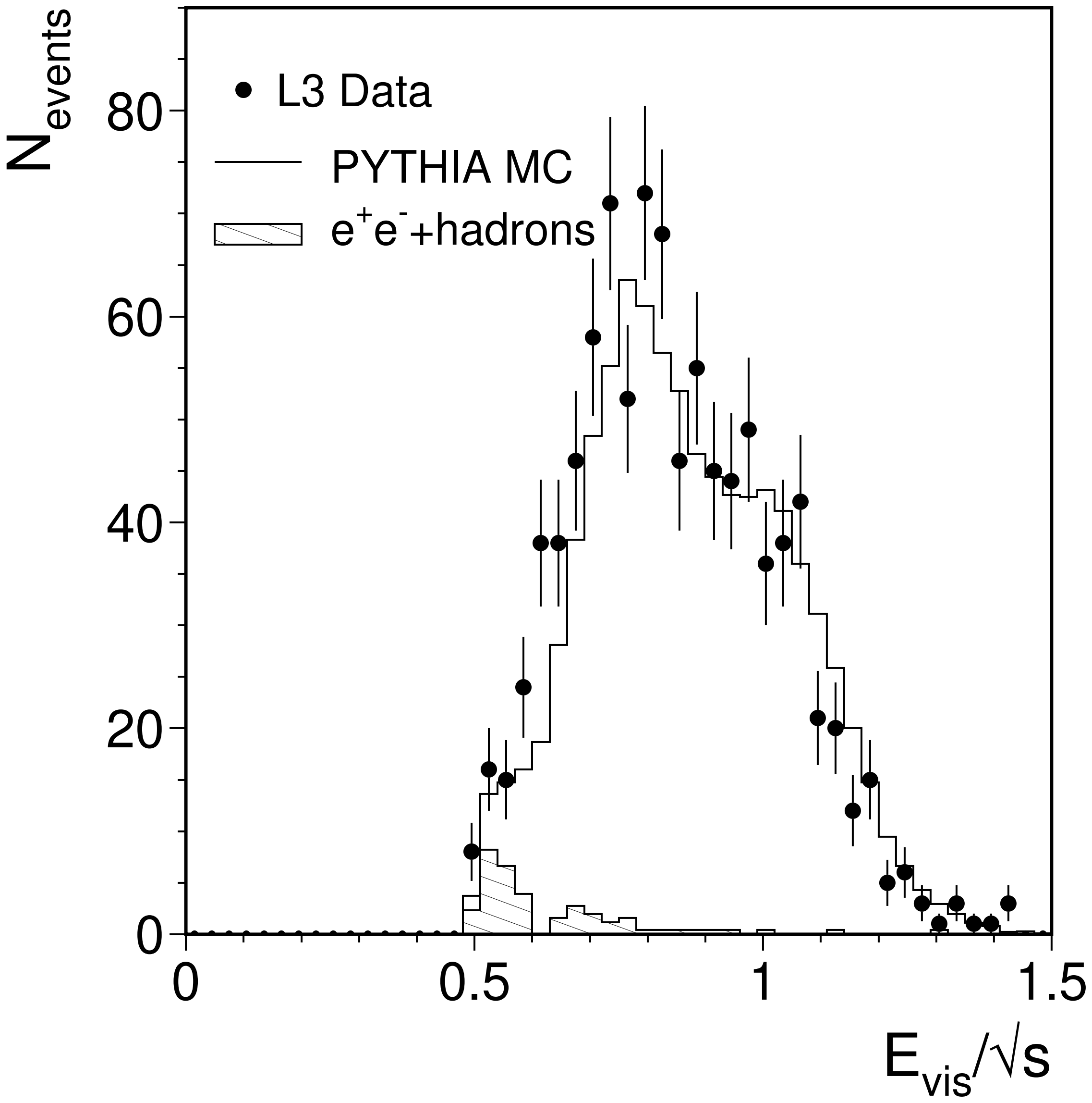

Figure 1: Visible energy after applying the hadronic selection for $\sqrt{s}$ =130 GeV events.

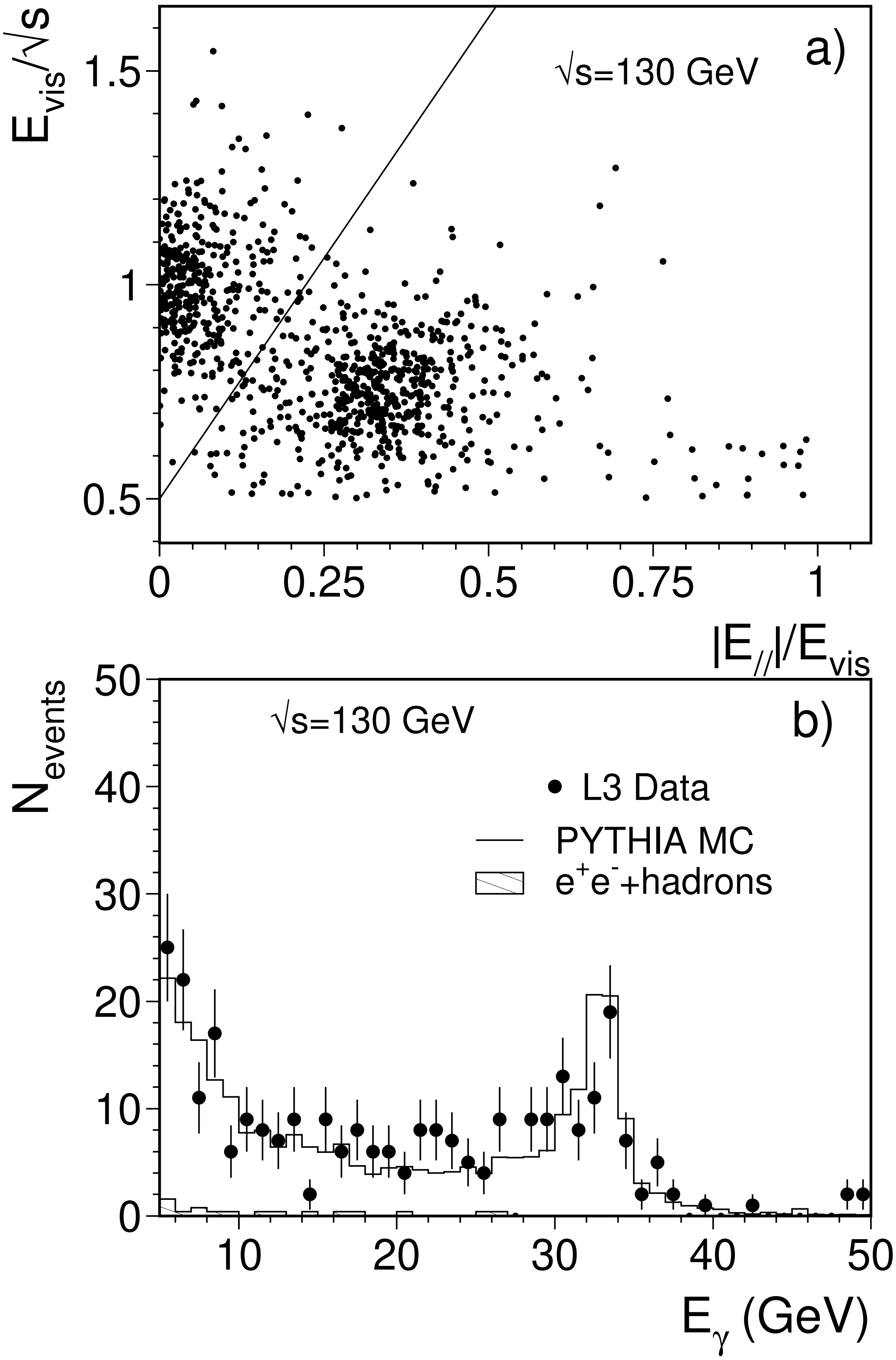

Figure 2: (a) Normalised visible energy shown as a function of the longitudinal imbalance for events at $\sqrt{s} = 130$ GeV. The well balanced events are clearly separated from the events with hard unobserved initial state radiation. (b) Energy distribution of the most energetic photon seen in the BGO calorimeter.

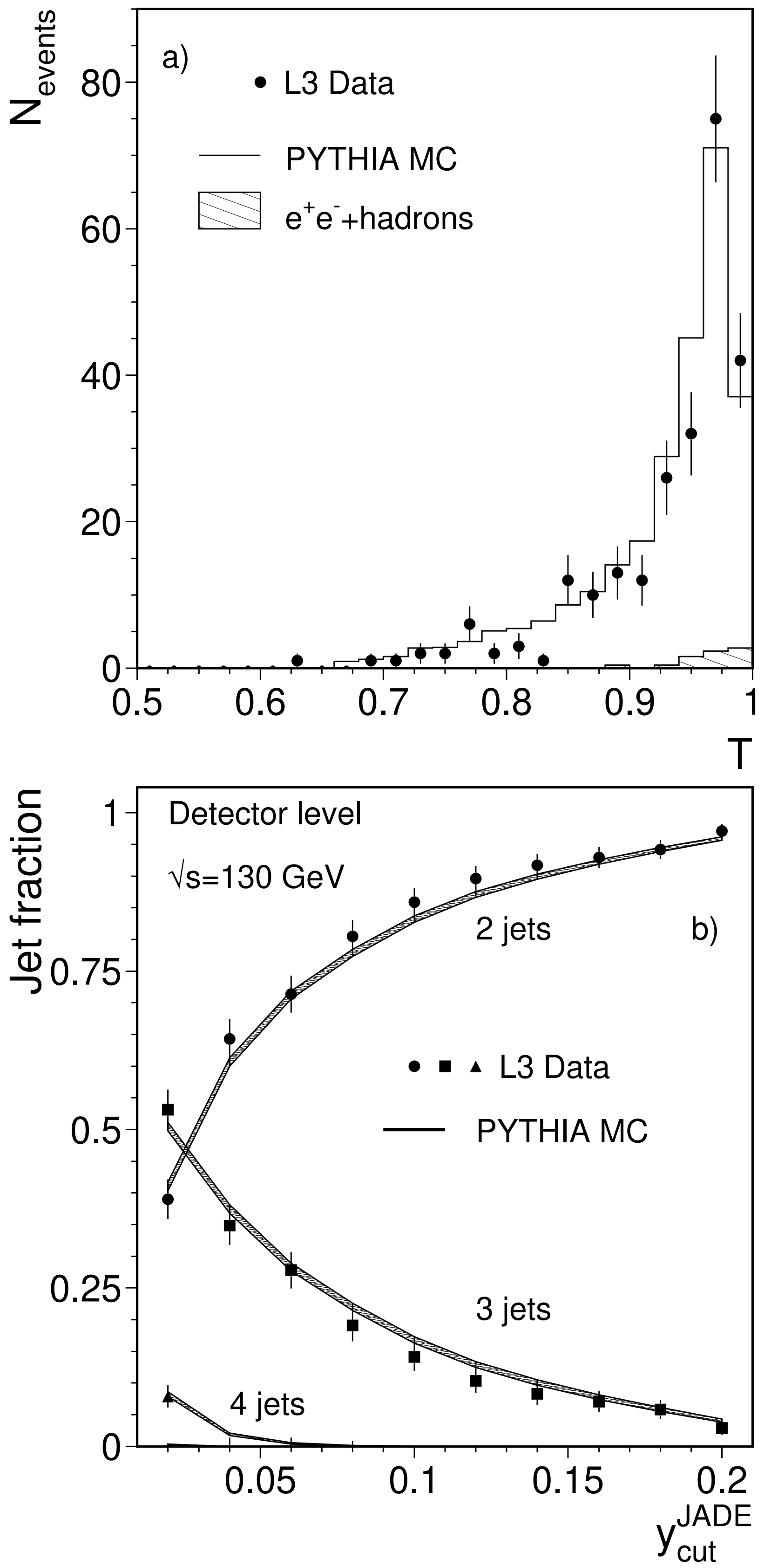

Figure 3: Distribution of thrust and jet rate as a function of y_{cut} at $\sqrt{s} = 130$ GeV compared to PYTHIA Monte Carlo. The band in 3(b) corresponds to the statistical error on the Monte Carlo.

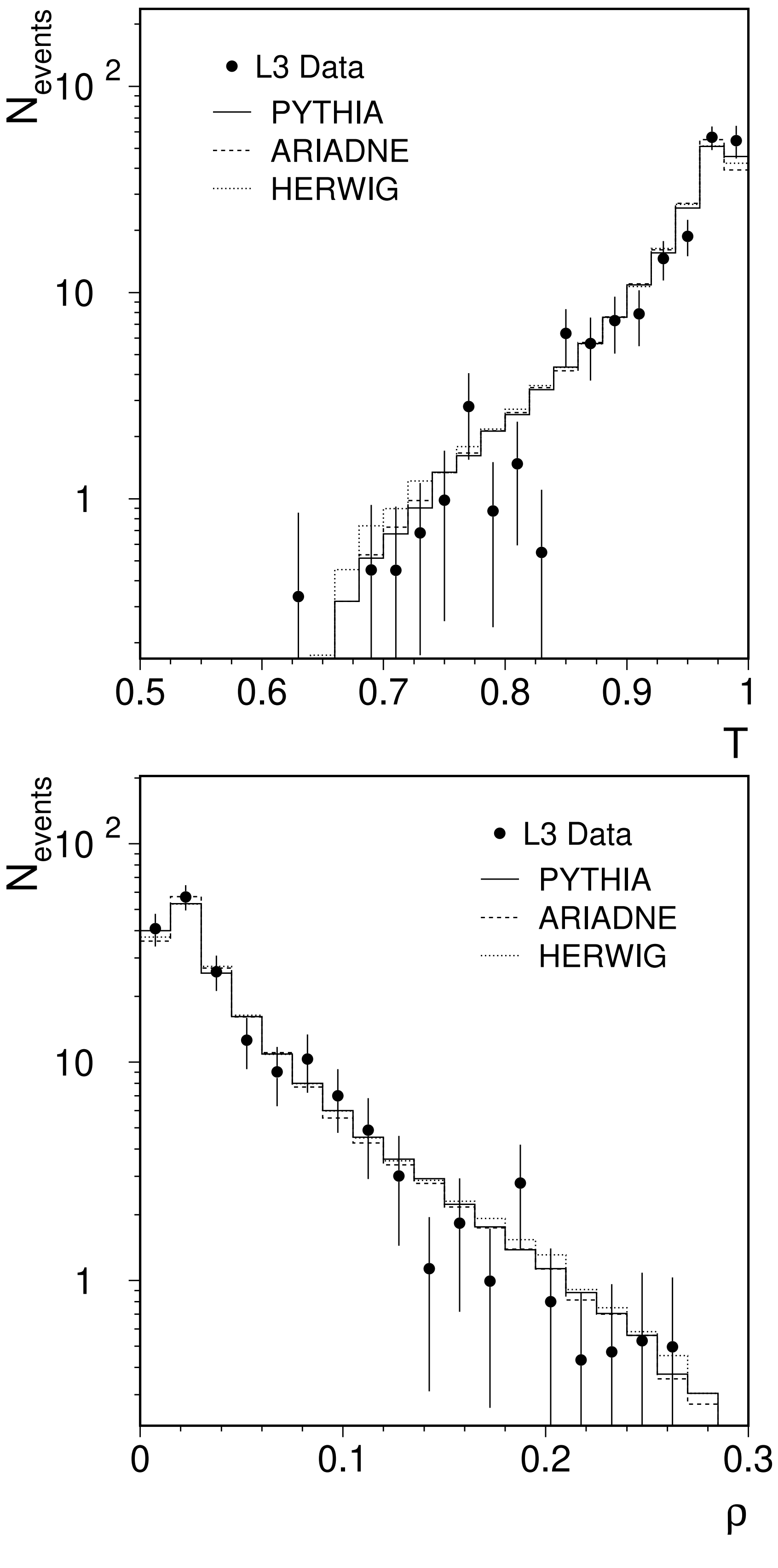

Figure 4: Distribution of thrust, T, and scaled heavy jet mass, ρ, after correction at $\sqrt{s}$ = 130 GeV in comparison with QCD model predictions. The experimental errors are only statistical.

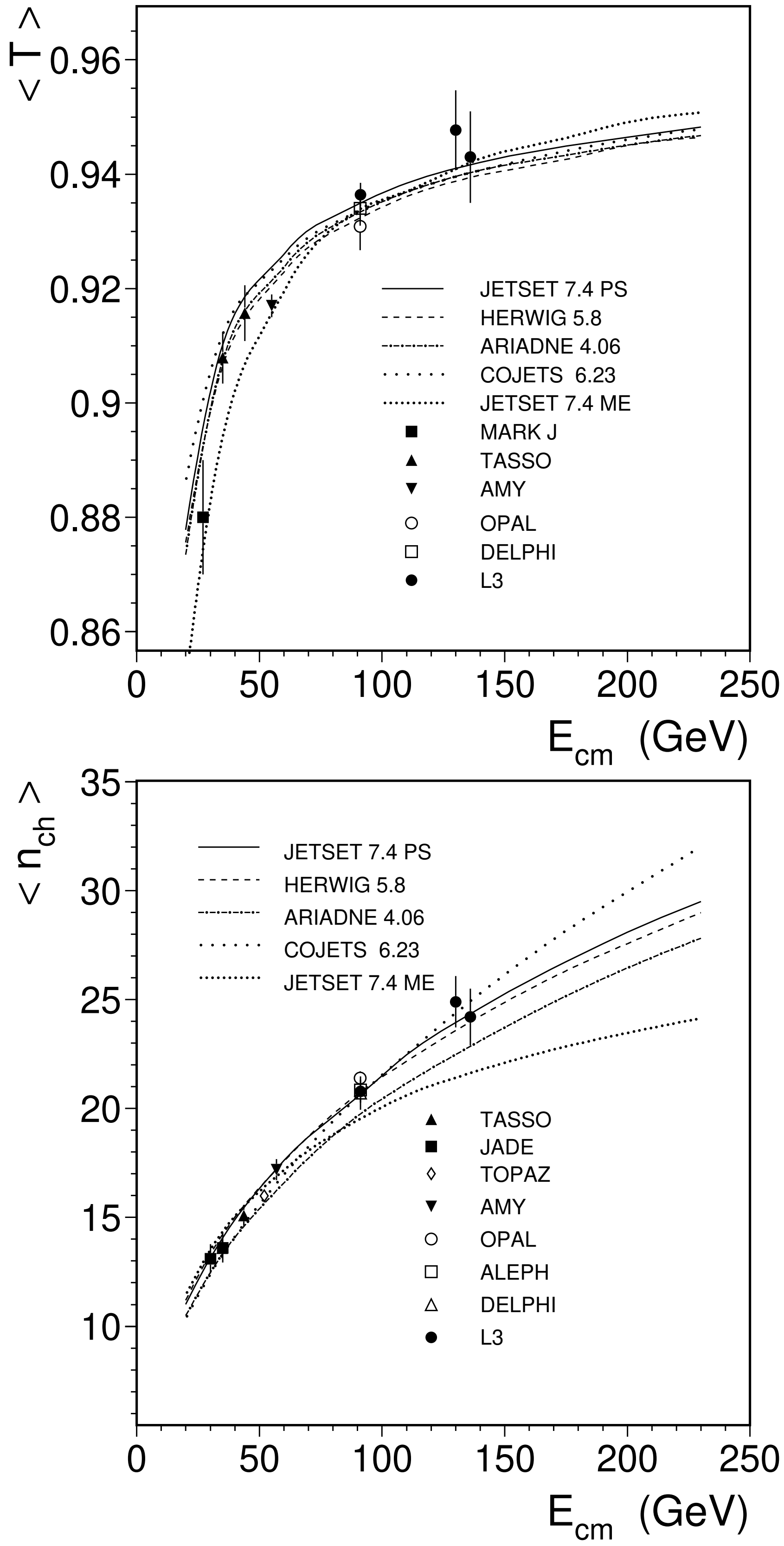

Figure 5: Distribution of mean thrust, $< T >$, and mean charge multiplicity, $< n_{ch} >$, as a function of the center-of-mass energy.

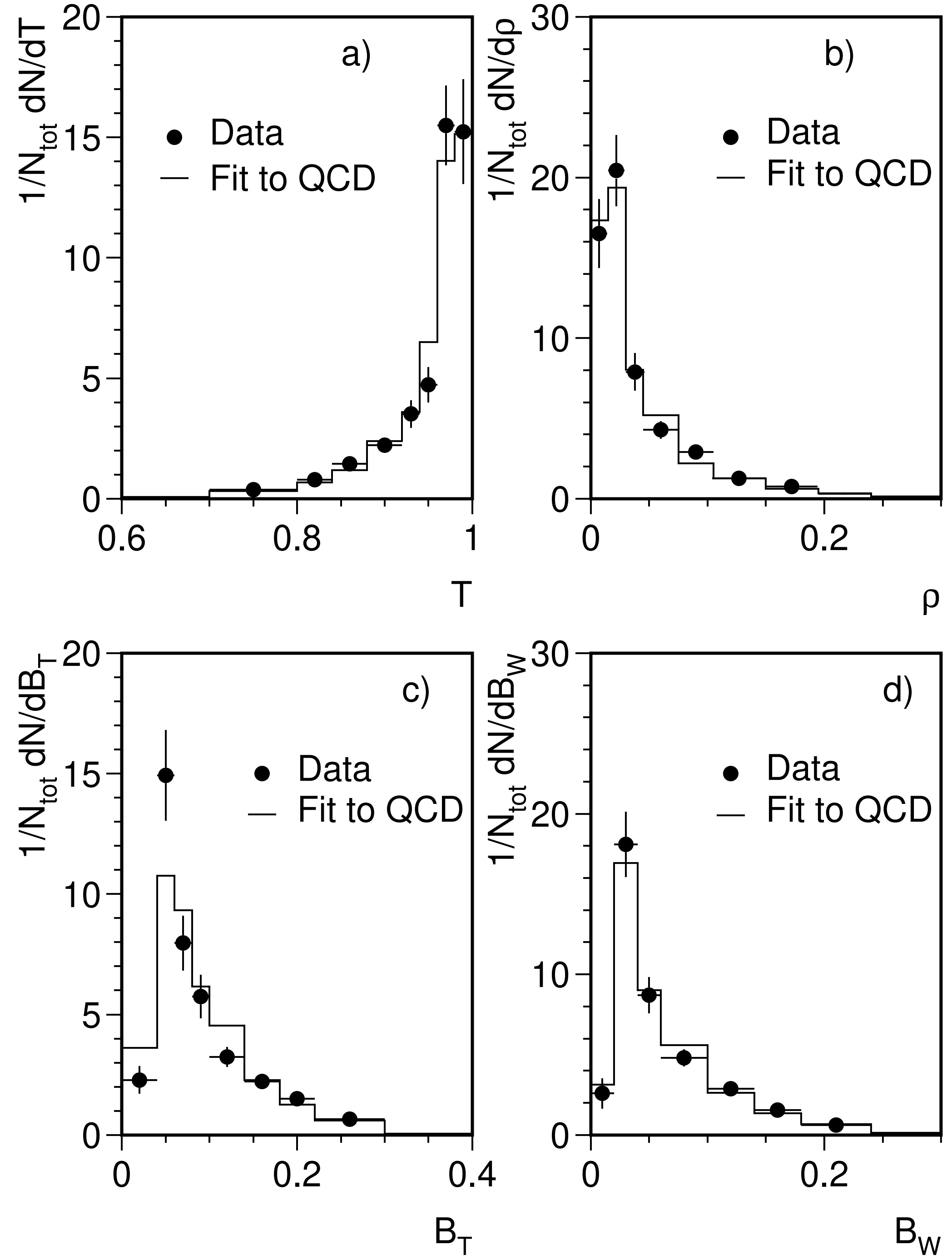

Figure 6: Measured distributions of thrust, T, scaled heavy jet mass, ρ, total, B_T, and wide, B_W, jet broadening in comparison with QCD predictions. The experimental errors include statistical and systematic uncertainties.